

New developments in laser-heated diamond anvil cell with in situ synchrotron x-ray diffraction at High Pressure Collaborative Access Team

Yue Meng, Rostislav Hrubak, Eric Rod, Reinhard Boehler, and Guoyin Shen

Citation: [Review of Scientific Instruments](#) **86**, 072201 (2015); doi: 10.1063/1.4926895

View online: <http://dx.doi.org/10.1063/1.4926895>

View Table of Contents: <http://scitation.aip.org/content/aip/journal/rsi/86/7?ver=pdfcov>

Published by the [AIP Publishing](#)

Articles you may be interested in

[A compact system for generating extreme pressures and temperatures: An application of laser-heated diamond anvil cell to inelastic X-ray scattering](#)

Rev. Sci. Instrum. **84**, 113902 (2013); 10.1063/1.4826497

[X-ray diffraction in the pulsed laser heated diamond anvil cell](#)

Rev. Sci. Instrum. **81**, 113902 (2010); 10.1063/1.3499358

[Portable laser-heating stand for synchrotron applications](#)

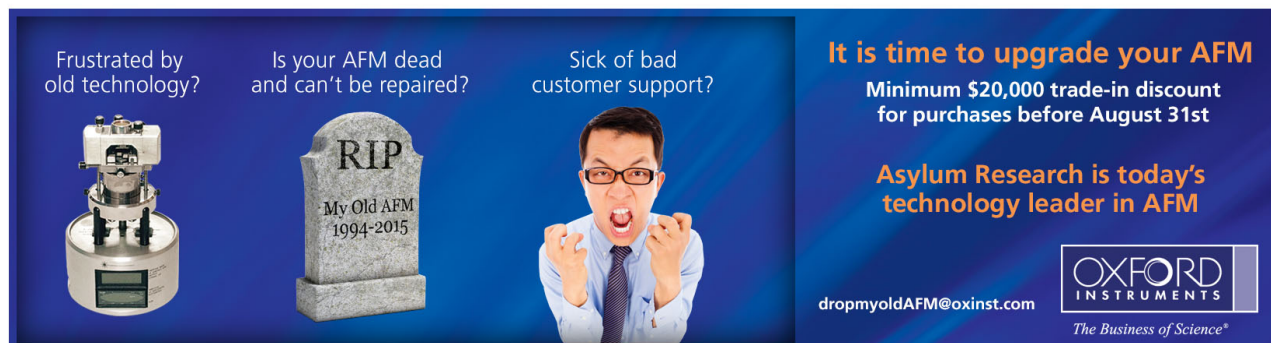
Rev. Sci. Instrum. **80**, 045103 (2009); 10.1063/1.3115183

[In situ laser heating and radial synchrotron x-ray diffraction in a diamond anvil cell](#)

Rev. Sci. Instrum. **78**, 063907 (2007); 10.1063/1.2749443

[Construction of laser-heated diamond anvil cell system for in situ x-ray diffraction study at SPring-8](#)

Rev. Sci. Instrum. **72**, 1289 (2001); 10.1063/1.1343869



Frustrated by old technology?

Is your AFM dead and can't be repaired?

Sick of bad customer support?

It is time to upgrade your AFM

Minimum \$20,000 trade-in discount for purchases before August 31st

Asylum Research is today's technology leader in AFM

dropmyoldAFM@oxinst.com

OXFORD
INSTRUMENTS
The Business of Science®

New developments in laser-heated diamond anvil cell with *in situ* synchrotron x-ray diffraction at High Pressure Collaborative Access Team

Yue Meng,¹ Rostislav Hrubyak,¹ Eric Rod,¹ Reinhard Boehler,² and Guoyin Shen¹

¹HPCAT, Geophysical Laboratory, Carnegie Institution of Washington, Argonne, Illinois 60565, USA

²Geophysical Laboratory, Carnegie Institution of Washington, Washington, DC 20015, USA

(Received 6 April 2015; accepted 28 June 2015; published online 17 July 2015)

An overview of the *in situ* laser heating system at the High Pressure Collaborative Access Team, with emphasis on newly developed capabilities, is presented. Since its establishment at the beamline 16-ID-B a decade ago, laser-heated diamond anvil cell coupled with *in situ* synchrotron x-ray diffraction has been widely used for studying the structural properties of materials under simultaneous high pressure and high temperature conditions. Recent developments in both continuous-wave and modulated heating techniques have been focusing on resolving technical issues of the most challenging research areas. The new capabilities have demonstrated clear benefits and provide new opportunities in research areas including high-pressure melting, pressure-temperature-volume equations of state, chemical reaction, and time resolved studies. © 2015 AIP Publishing LLC. [<http://dx.doi.org/10.1063/1.4926895>]

I. INTRODUCTION

Laser-heated diamond anvil cell (LHDAC) coupled with the *in situ* synchrotron x-ray diffraction (XRD) is a unique and powerful experimental technique for studying a broad range of material properties under extreme conditions up to megabars of pressure and several thousand degrees Kelvin of temperature. Over the last decade, this technique has evolved into a routinely used and productive experimental method at synchrotron beamlines, leading to numerous major scientific advances and a large expansion of high-pressure research in physics, chemistry, geoscience, and materials science.^{1–8} One of the main applications of continuous wave laser heating (CWLH) has been the use of high temperature for overcoming kinetic barriers to phase transformation and for enabling new materials synthesis at high pressure. Thus, technical developments have emphasized long-term system stability with heating duration in a typical experiment lasting from minutes to hours.^{9,10,15} Such long term temperature stability of the CWLH has made possible many studies of phase transitions,¹¹ materials synthesis,⁶ and sample annealing for equations of state (EOS) measurement.¹² High pressure melting studies using synchrotron x-ray have been complicated by several issues including melt containment, temperature gradient, chemical reactions, and maintaining the exact alignment of the melt volume and the x-ray beam. Pressure-volume-temperature (P-V-T) EOS study is another challenging area that requires the exact alignment of heating, x-ray and temperature measurement positions at all the time during the experiment, which is not always guaranteed in the conventional systems commonly used at synchrotron beamlines.

In recent years, modulated pulse laser heating is being increasingly used for high pressure research. From technical perspective, LHDAC in short time scale has several potential advantages. (1) It reduces the exposure of cell assembly to high temperature conditions. This helps to maintain the

cell assembly's structure integrity and stability, thus improves the consistency and quality of experimental measurements and increases the potential for reaching higher pressure and temperature. (2) The short heating duration helps to suppress thermally activated chemical diffusion and reaction. (3) Heating at short time scales and improved temporal resolution of temperature measurement have been very useful for high-pressure melting studies, and studies of phase transition dynamics under high pressure. From the scientific perspective, current 3rd and 4th generation synchrotron sources provide opportunities to explore a wide range of physical and chemical phenomena occurring in increasingly short time scales down to femtosecond level. There is a need for LHDAC development to match the time scale of the light sources.

Our technical development objective in recent years has been to advance the experimental capabilities that address specific issues in the most challenging areas of high pressure research, specifically high-pressure melting and P-V-T EOS. In this paper, we summarize new techniques established at the beamline 16-ID-B in recent years, including (1) on-line heating-spot size adjustment to provide effective and uniform heating on various-sized samples in the diamond anvil cell; (2) mirror pinhole setup to allow direct viewing of the temperature sampling area relative to the heating area and x-ray beam, and online adjustment to ensure the ideal alignment for reliable experimental measurements; and (3) modulated laser heating technique synchronized with XRD, temperature measurement, and thermal imaging for high pressure melting and time-resolved studies of phase transition dynamics under high PT conditions.

II. SYSTEM OVERVIEW

The integrated system of LHDAC with *in situ* XRD is located at High Pressure Collaborative Access Team's

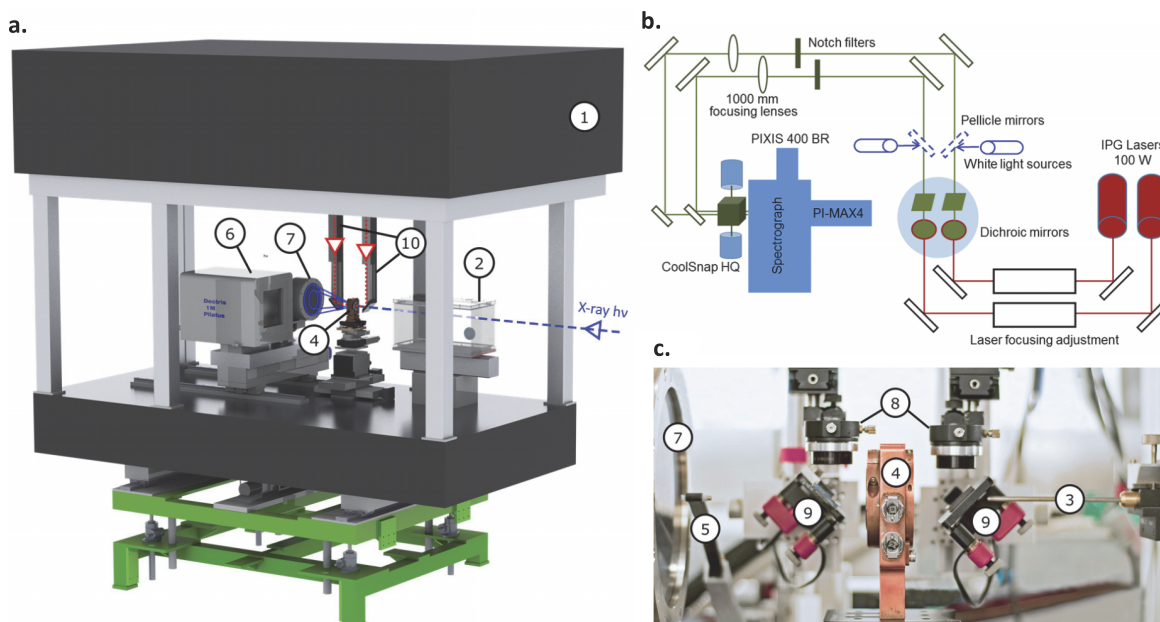


FIG. 1. The integrated system of laser-heated DAC with *in situ* XRD. (a) A computer-aided-design (CAD) drawing of the laser heating experiment table in 16-ID-B, (b) a schematic drawing of the optical system on the top experiment table (labeled as ①), and (c) an image of the setup around DAC. The numbered label ② denotes KB mirrors for XR focusing, ③ XR clean-up pinhole, ④ diamond anvil cell, ⑤ XR beam stopper, ⑥ Pilatus 1M XR detector, ⑦ MAR CCD XR detector ⑧ the apochromatic objective lenses, ⑨ coated amorphous carbon mirrors, and ⑩ movable holders for laser heating system components ⑤ and ⑨.

(HPCAT) monochromatic angle dispersive x-ray diffraction station 16-ID-B (Figure 1). Upgraded in 2009, 16-ID-B's x-ray source provides undulator-based radiation ranging from 12 to 42 KeV. The incident x-ray beam is first focused by a pair of 200 mm-long Kirkpatrick-Baez (KB) mirrors to 3–8 μm . The beam is then spatially filtered through a clean-up pinhole to remove tailing radiation intensity, before reaching the sample position.

The online laser heating system features double-sided heating in continuous-wave mode or in modulation mode and *in situ* temperature measurements, independently on both sides. The heating laser spot size can be varied remotely from 4 to >60 μm in flat top area and from 9 to >120 μm in FWHM (flat top area is defined as >90% Gaussian laser peak intensity). The mirror-pinhole at the entrance of the spectrometer allows the experimenters to observe from where temperature is measured relative to the total area of the heated spot for precise alignment and to ensure experiment data quality. *In situ* XRD is achieved by using a pair of x-ray transparent mirrors for infrared (IR) laser delivery and temperature measurement. The diffraction patterns are recorded with the interchangeable MAR CCD, MAR imaging plate, or a Pilatus 1M detectors. Any of the two of the detectors may be attached to a motorized translation stage to enable fast on-line detector switching.

A. Heating components and optics

The heating system includes two 100 W IR (1064 nm) Ytterbium fiber lasers for heating DAC from both sides independently. In each laser's beam path, there is a laser beam expander for controlling the laser beam diameter and divergence to achieve a desired heating spot size with a flat temperature profile, a dichroic mirror which reflects the IR laser beam and transmits visible light, an apochromatic objective

lens (77 mm focal length, chromatic-aberration corrected for visible and 1064 nm) for laser beam and imaging focusing, and a 4 mm thick amorphous carbon mirror with protected silver coating for reflecting IR laser beams to pass through the opposing diamond anvils for sample heating.

B. Temperature measurement

Temperatures are determined by fitting Planck radiation function (1) to the black-body radiation¹³ (600 nm–800 nm) from a spatially selected area (4 μm in diameter) on the heated sample,

$$I_{\lambda} = \frac{c_1 \epsilon(\lambda) \lambda^{-5}}{\exp(c_2/\lambda T) - 1}, \quad (1)$$

where I_{λ} is the spectral intensity, ϵ emissivity, λ wavelength, T temperature, $c_1 = 2\pi hc = 3.7418 \times 10^{-16} \text{ W m}^2$, and $c_2 = hc/k = 0.014 388 \text{ mK}$. Thermal radiation from heated sample is collected from both sides of DAC by the same carbon mirrors and objective lenses as used for delivering heating laser. The thermal radiation from each side of the sample then passes through dichroic mirror and notch-filters to remove any IR and is focused by achromatic lens (FL = 1000 mm) onto one of the two respective pinholes on the entrance of the imaging spectrograph^{14,15} (SP2560, Princeton Instruments). We implemented the mirror pinhole concept by Reinhard Boehler *et al.*¹⁶ This allows the spectrograph entrance pinholes which define the temperature measurement areas on sample being observed together with the heated sample itself. The imaging spectrograph includes two area detectors, a back-illuminated CCD detector (PIXIS 400BR, Princeton Instruments) and a time-gated intensified electron-multiplying CCD detector (em-ICCD, PI-MAX4, Princeton Instruments),

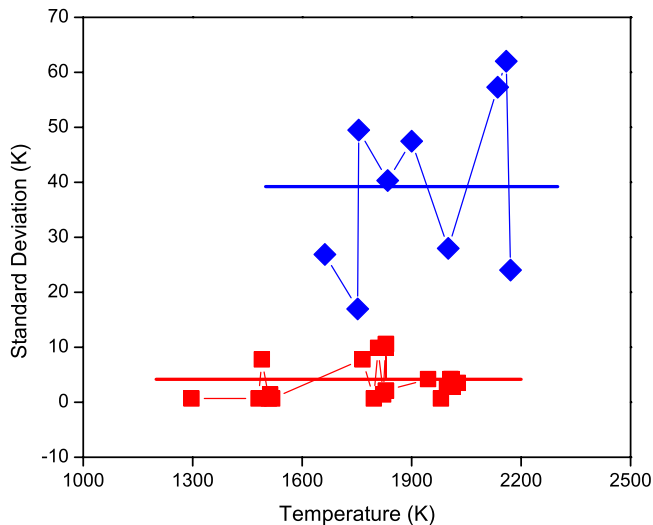


FIG. 2. A comparison of heating stability using lamp-pumped laser (blue symbols) and using diode-pumped fiber laser (red symbols). The experiments were conducted in megabar pressure range with identical sample and cell assembly configuration.

which can be used interchangeably. The spectral ranges available on the detectors are 169 nm (300 G/mm grating) and 340 nm (150 G/mm grating) on the CCD detector, and 157 nm (150 G/mm grating) on the em-ICCD detector. The em-ICCD

detector can be electronically gated at the picosecond level and used for fast temperature measurement.

In continuous-wave laser heating, the replacement of the previously used lamp-pumped lasers¹⁵ by the diode-pumped fiber lasers has significantly improved the sample heating stability. Figure 2 shows the standard deviations of multiple measurements in a time period of 1–2 h in experiments of magnesium silicate post-perovskite study conducted under megabar pressure range using lamp-pumped laser (blue symbols) and using diode-pumped fiber laser (red symbols).

III. NEW CAPABILITIES

A. *In situ* heating spot size variation

In conventional laser heating systems used in most user facilities, the power of laser spot at the sample focus has a Gaussian radial distribution, typically fixed at 20–30 μm in FWHM. However, the sample sizes in DAC vary from a few to over 100 μm in the dimension normal to the laser beam. The small heating spot size causes temperature gradient inside the heated sample. Temperature gradient is problematic for some samples. For instance, temperature gradient in iron-containing silicates causes the iron to migrate and consequently changes the chemical composition of the sample and

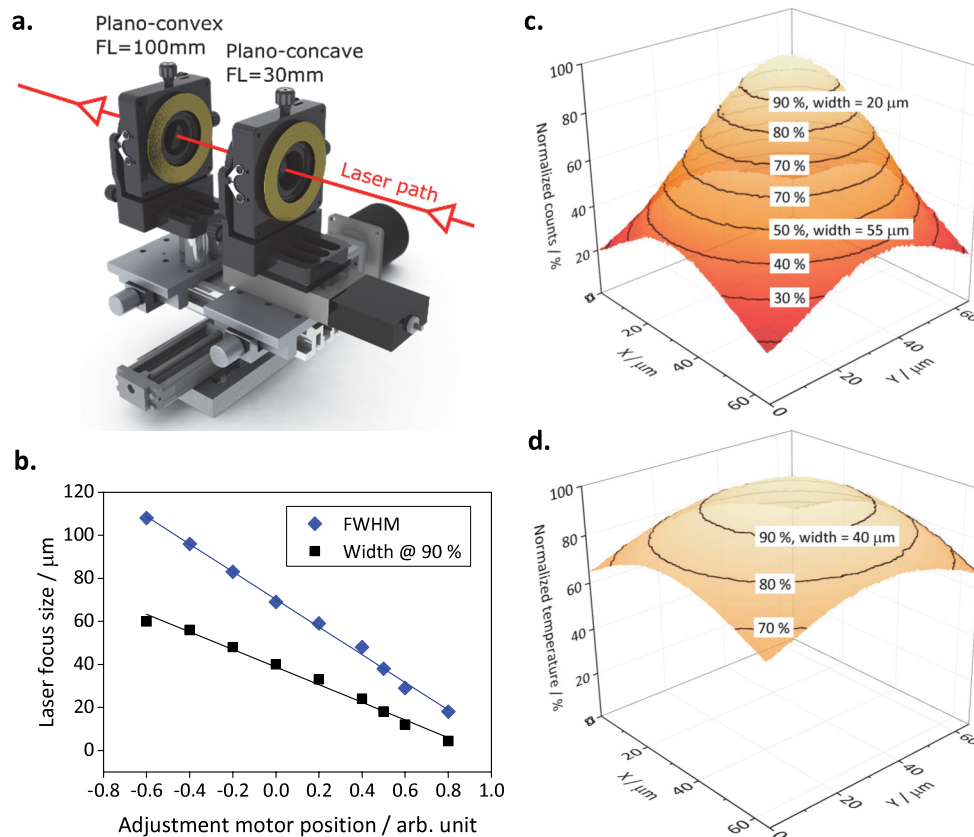


FIG. 3. (a) CAD drawing of the setup used for varying the size of the laser heating area. The concave and convex lenses are mounted on 2 Newport's LP-2A five axis lens positioners providing 5° of motion adjustment for coaxial alignment of the two lenses. The two linear stages are used to adjust the distance between the two lenses (focusing stage under the concave lens) and to move the whole unit in and out for alignment purpose. (b) Plot of the laser focus spot dimension, derived from measured thermal radiation intensity distribution, as a function of adjustment motor position. (c) A 3D plot of the measured thermal radiation distribution on a laser-heated area on a platinum foil (foil thickness ~ 10 nm), and (d) a 3D plot of the temperature distribution of the same heating spot, calculated using an approximation of the Stefan-Boltzmann law.

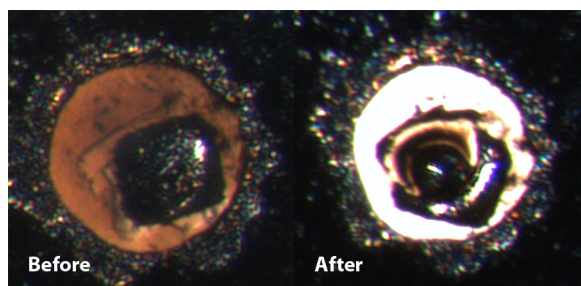


FIG. 4. Laser heating of a Mo sample at 60 GPa before and after melting using a heating spot size of $60\ \mu\text{m}$ in flat-top area.

affects the experimental result. Conversely, if the sample dimensions are very small ($<10\ \mu\text{m}$), a smaller laser spot may be required for effective heating. In order to meet the diverse heating requirements, we have developed a system which allows the on-line remote control and viewing of the laser spot size and consequently temperature gradient in the samples during an actual heating experiment.

The *in situ* heating spot size control is achieved using a system with a Galilean beam expander design shown in Figure 3(a). It consists of a 30-mm concave lens and a 100-mm convex lens mounted on a linear stage for varying the distance between the two lenses, which changes both the laser beam size and divergence and consequently changes the focus size.

The focus size, flat-top dimension (spot width at 90% intensity), and FWHM, as a function of the linear stage motor position, are shown in Figure 3(b). The focus size of the resulting laser spot decreases with increasing distance between the two lenses. The heating spot sizes in 3(b) are determined from measured thermal radiation distribution of actual heating spots, one such example is shown in 3(c). The flat-top area focus sizes from $4\ \mu\text{m}$ to $>60\ \mu\text{m}$ have been achieved and used in user experiments (Figures 4 and 6).

B. Mirror pinhole setup

The alignment of heating laser, x-ray beam and temperature measurement areas is a key to a successful *in situ* measurement. Previously, the temperature sampling area could not be viewed directly and the users were not provided

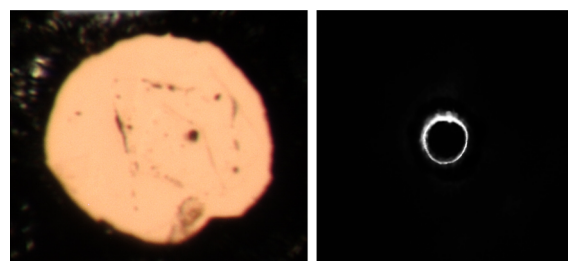


FIG. 6. Laser heating of a $5\ \mu\text{m}$ Pt sample. Left: before heating, sample is encapsulated in single crystal MgO prepared by Karandikar. Right: laser heated sample viewed through the mirror pinhole system. The center black area is an image of the actual pinhole at the spectrograph entrance for collecting thermal radiation. The image shows that the temperature sampling area is aligned with the heating area of the sample.

with an *in situ* observation of the correct system alignment. However, for studies requiring exact alignment between XRD, heating spot and temperature measurements, e.g., P-V-T EOS, and for samples with dimensions $<10\ \mu\text{m}$, $1\ \mu\text{m}$ accuracy is essential. It is generally known that the instability level for typical mechanical system used at beamlines can result in a misalignment of several microns between the heating laser spot, x-ray beam, and temperature measurement area. Such misalignment may lead to systematic measurement errors and can be detrimental for measurement at very high pressures where sample features can typically be $<10\ \mu\text{m}$. Mirror pinhole setup¹⁶ addresses this issue and allows experimenters to view the pinhole position relative to heating and XRD spots and make proper adjustment if needed.

The mirror pinhole setup in the laser heating system at 16-ID-B is demonstrated in Figure 5. A CAD drawing of the setup is shown in (a) and a schematic illustration in (b). In our system, we use an aluminum plate with a mirror-quality surface. Two round ($50\ \mu\text{m}$ diameter) pinholes are located in the central area of the aluminum plate, vertically separated by 6 mm. The mirror pinhole plate is mounted at the spectrograph entrance. The spectrographs collect the thermal radiation which goes through each of the pinholes, one for each of respective side of a heated sample. The mirror serves for reflecting the image of sample, which may either be the thermal image of the sample or the fluorescence spot of x-ray beam used for alignment. Cube beam splitters are

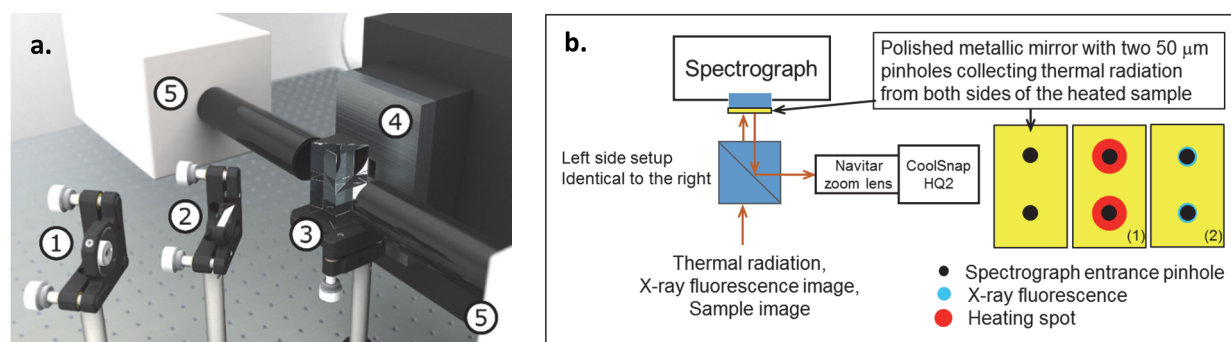


FIG. 5. Mirror pinhole system at 16-ID-B: (a) a CAD drawing of the setup and (b) a schematic diagram. The numbered labels in (a) denote reflection mirrors ① and ② for visible light signals from the two sides of the heated sample, beam splitter cubes ③, mirror pinhole holder ④, and CoolSnap HQ2 cameras ⑤. In the schematic diagram, only the beam splitter and viewing system on the right side are shown. Camera display of pinhole alignment with heating spot is shown in (1) and with x-ray fluorescence in (2).

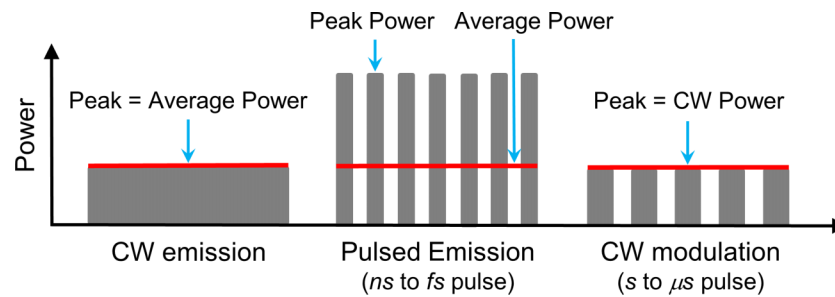


FIG. 7. A comparison of power output of CW laser, pulsed laser, and modulated CW laser. The power distribution of the pulsed emission is typically close to Gaussian, not the squared shape as schematically shown. The pulse shape from a CW modulation is defined by a power ramp up, an overshoot immediately after the ramp up, a period of constant power, and a power ramp down. The square shape as schematically shown can be achieved through electro-optical modulation which will be presented in a separate paper.

used for collecting the light reflected from the mirror pinhole surface to be used in a viewing system (focusing objective, Navitar; CoolSNAP HQ2 camera, Princeton Instruments). This setup allows the experimenters to directly observe the pinhole position relative to the heating spot, sample, fluorescence spot of x-ray beam, thus ensuring the exact alignment. As shown in Figure 6, when heating a 5- μm Pt sample, the exact alignment is achieved for a reliable temperature measurement.

C. Modulated pulse laser heating and the synchronization with XRD

Pulse laser heating can be achieved using a pulsed laser or a CW laser in modulation mode. However, due to the differences in power output, the two types of lasers are targeted for different applications. The power output of CW laser, pulsed laser, and CW modulation is illustrated in Figure 7.

Pulsed lasers release laser energy in a very short time scale of each pulse duration (femtoseconds to nanoseconds); therefore, the peak power of the pulses is much higher than that of a CW laser with the same amount of energy. Pulses in CW modulation, on the other hand, are generated through laser emission control, and its peak power is the same as the CW laser output of same energy level. The pulse duration of CW modulation ranges from microseconds to seconds with constant power level, offering opportunities for a much wider range of applications in research of structural properties including phase transition, melting, and P-V-T EOS.

At HPCAT, we focus on developing techniques for applications using CW modulation. These applications involve single laser pulse generation (IPG lasers) synchronized with temperature (CCD and em-ICCD) and XRD (Pilatus 1M) measurements.

Our current setup is illustrated schematically in Figure 8. As shown in the figure, the trigger pulses for laser, temperature measurement, XRD, and viewing camera recording are generated by a pulse generator (Berkeley Nucleonics Corporation, BNC Model 505-8C). The pulse duration and frequency for each device and the synchronization of all devices are controlled by EPICS software with MEDM graphical user interface and displayed on a digital phosphor oscilloscope (Tektronix TDS 3054 C).

In Figure 9, we show a few commonly used combinations of triggering pulses and their synchronization: single pulse heating with synchronized temperature and XRD measurements in (a) and (b) and single pulse (c) and ramp (d) heating with synchronized multiple temperature and XRD measurements for time-resolved studies.

Modulated pulse laser heating offers promising opportunity for high pressure melting research. Figure 10 shows XRD patterns of uranium at high pressure captured before, during, and after a laser heating pulse using the triggering combination shown in Figure 9(b) with laser heating pulse width 1 second, temperature CCD pulse width 0.8 s, and XRD pulse width 0.8 s. This triggering combination allows to record the data from a complete sequence of sample conditions with one press of a button.

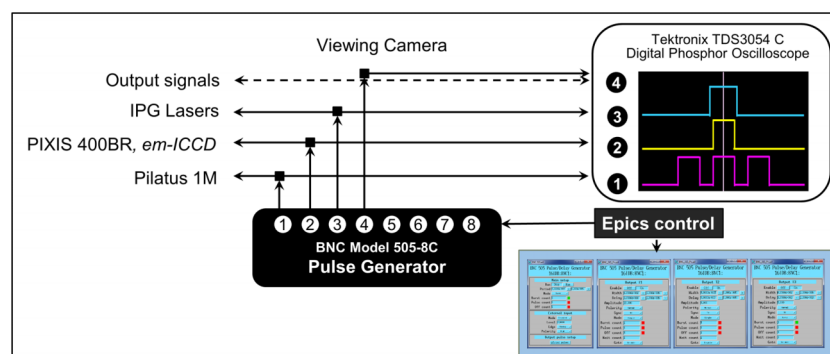


FIG. 8. A schematic illustration of the setup currently used at HPCAT for pulse generation and synchronization. The oscilloscope displays a single laser pulse (channel 3) synchronized with a temperature pulse (channel 2) and XRD pulses (channel 1). Channel 4, typically used for displaying either input pulses for viewing camera or the output pulses from detectors, is not shown on the oscilloscope display.

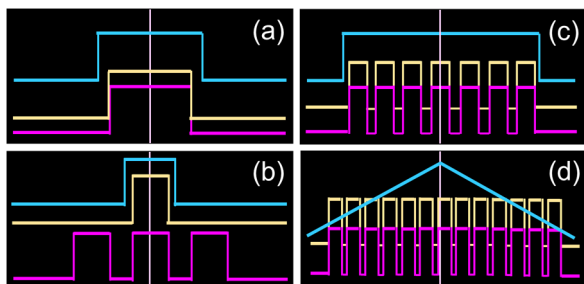


FIG. 9. A few commonly used synchronizations of modulated pulse heating (cyan) with *in situ* T (yellow) and XRD (magenta) measurements.

D. Synchronized fast thermal imaging and application to melting studies

In CW laser heating, the mirror pinhole setup provides a reliable way to ensure the alignment of temperature measurement area with heating spot by directly comparing the images of pinhole and heating spot (thermal radiation) on camera's monitor. Due to the short heating duration, in pulse heating, especially with single pulse heating, the capture of the thermal radiation image needs to be fast and synchronized with laser pulse. This is achieved by gating the thermal imaging camera in synchronization with the heating pulses. The imaging system currently in use allows the recording of thermal images 20 ms apart. An example of such synchronization is shown in Figure 11(a). The capture of the thermal image of a heating spot within a heating pulse duration is essential for checking the alignment of the heating spot with the temperature measurement pinhole. In Figure 11(b), the image on the left was captured during a heating pulse showing a slight misalignment between the heating spot and the pinhole. To align the two, laser position adjustment was made, and the image on the right shows improved alignment.

The synchronized fast thermal imaging in combination with the mirror pinhole setup discussed in Section III B ensures the exact alignment of heating spot, temperature, and XRD measurements in single pulse laser heating experiments.

Figure 12 shows the result of temperature measurements in a Mo melting experiment under very high pressure using single pulse laser heating. Mo samples were loaded between single crystal MgO thermal insulation layers of identical thicknesses. The heating and measurements were conducted using

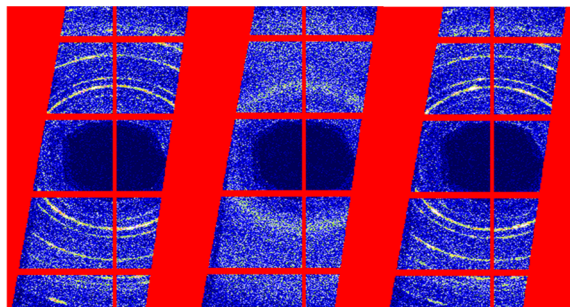


FIG. 10. Melting of uranium at high pressure captured using the pulse synchronization displayed in Figure 9(b), before (left), during (middle), and after (right) the heating pulse (in collaboration with Hyunhae Cynn).

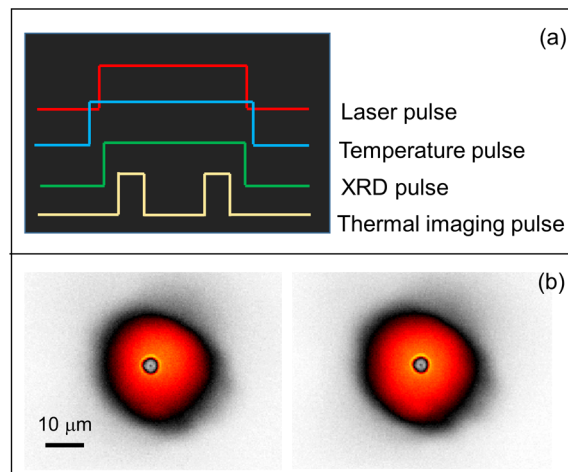


FIG. 11. (a) Synchronization of thermal images with laser heating pulse. In (b), images of a single pulse heating spot relative to pinhole position before (left) and after (right) laser position adjustment were made.

a series of discrete single laser pulses measurements up to 6000 K with melting occurring at around 4100 K. The temperature difference from the two sides of the sample is small with an averaged absolute value of 46 K before melting and 95 K

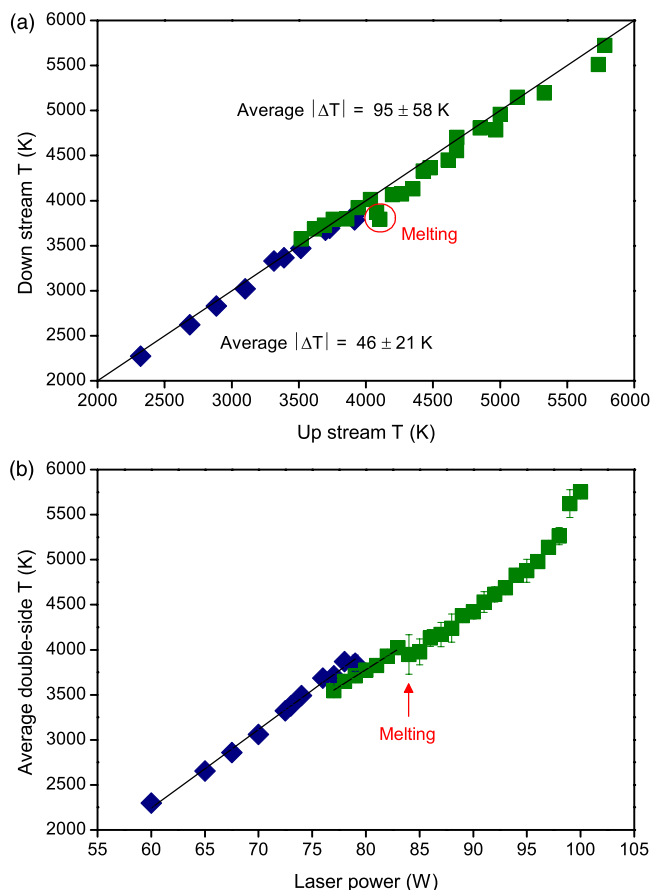


FIG. 12. Double-sided temperature measurements of a laser-heated Mo sample in DAC. Each data point was measured within a 10 ms laser pulse duration. The sample is insulated with single crystal MgO of identical thickness on both sides. The two symbols represent measurements from two different heating locations on the same sample. Please note that the criteria for melting point determination, not based on the discontinuities in the plots, will be presented elsewhere.

after melting. In addition to the small temperature difference, the average temperature of the two sides increases linearly with laser power before melting. Melting induces some visible instability when compared with the data in the solid phase, the increased temperature difference as shown in Figure 12(a), and the slight nonlinearity in the temperature-power relationship as shown in Figure 12(b).

This result demonstrates the benefits of reliable alignment using the mirror pinhole setup and the synchronized thermal imaging, as well as the short heating duration. The short heating duration minimizes the effect of high temperature and melting on cell assembly stability, and this allows the temperatures of the melt phase being measured up to near 6000 K.

IV. SUMMARY

In the past a few years, several new capabilities in both CW and modulation pulse laser heating areas have been developed and implemented at HPCAT. These capabilities allow users to have *in situ* control of heating spot size, to directly observe temperature sampling position relative to heating spot, and to ensure precise alignment. With an added time dimension, laser heating synchronized with temperature and XRD measurements at a microsecond time scale have been achieved. These new capabilities provide opportunities for challenging high-pressure research including high-pressure melting and P-V-T equation of state measurements.

ACKNOWLEDGMENTS

We would like to thank Curtis Kenney-Benson, Stanislav Sinogeikin, and Arunkumar Bommannavar for technical support, and Amol Karandikar for discussions and suggestions. This work was performed at HPCAT (Sector 16), Advanced

Photon Source (APS), Argonne National Laboratory. HPCAT operations are supported by DOE-NNSA under Award No. DE-NA0001974 and DOE-BES under Award No. DE-FG02-99ER45775, with partial instrumentation funding by NSF. The Advanced Photon Source is a U.S. Department of Energy (DOE) Office of Science User Facility operated for the DOE Office of Science by Argonne National Laboratory under Contract No. DE-AC02-06CH11357. Reinhard Boehler is supported by EFree, an Energy Frontier Research Center funded by DOE-BES.

- ¹W. A. Bassett, *Rev. Sci. Instrum.* **72**, 1270 (2001).
- ²L. Liu, *Geophys. Res. Lett.* **1**, 277, doi:10.1029/GL001i006p00277 (1974).
- ³R. Boehler, *Nature* **363**, 534 (1993).
- ⁴G. Y. Shen, V. B. Prakapenka, M. L. Rivers, and S. R. Sutton, *Phys. Rev. Lett.* **92**, 185701 (2004).
- ⁵S. H. Shim, T. S. Duffy, R. Jeanloz, and G. Y. Shen, *Geophys. Res. Lett.* **31**, L10603, doi:10.1029/2004GL019639 (2004).
- ⁶B. Lavina, P. Dera, E. Kim, Y. Meng, R. T. Downs, P. F. Weck, S. R. Sutton, and Y. Zhao, *Proc. Natl. Acad. Sci. U. S. A.* **108**, 17281 (2011).
- ⁷L. Zhang, Y. Meng, W. G. Yang, L. Wang, W. L. Mao, Q. S. Zeng, J. S. Jeong, A. J. Wagner, K. A. Mkhoyan, W. J. Liu, R. Q. Xu, and H. K. Mao, *Science* **344**, 877 (2014).
- ⁸W. L. Mao, Y. Meng, G. Y. Shen, V. B. Prakapenka, A. J. Campbell, D. H. Heinz, J. Shu, R. Caracas, R. E. Cohen, Y. Fei, R. J. Hemley, and H. K. Mao, *Proc. Natl. Acad. Sci.* **102**, 9751 (2005).
- ⁹V. B. Prakapenka, A. Kubo, A. Kuznetsov, A. Laskin, O. Shlurikhin, P. Dera, M. L. Rivers, and S. R. Sutton, *High Pressure Res.* **28**, 225 (2008).
- ¹⁰A. J. Campbell, *Rev. Sci. Instrum.* **79**, 015108 (2008).
- ¹¹P. Dera, G. J. Finkelstein, T. S. Duffy, R. T. Downs, Y. Meng, V. B. Prakapenka, and S. Tkachev, *Phys. Earth Planet. Inter.* **221**, 15 (2013).
- ¹²S. M. Dorfman, Y. Meng, V. B. Prakapenka, and T. S. Duffy, *Earth Planet. Sci. Lett.* **361**, 249 (2013).
- ¹³D. L. Heinz and R. Jeanloz, in *High Pressure Researches in Mineral Physics*, edited by H. M. Manghnani and Y. Syono (American Geophysical Union, Washington, DC, 1987).
- ¹⁴G. Y. Shen, M. L. Rivers, Y. Wenge, and S. R. Sutton, *Rev. Sci. Instrum.* **72**, 1273 (2001).
- ¹⁵Y. Meng, G. Y. Shen, and H. K. Mao, *J. Phys.: Condens. Matter* **18**, S1097 (2006).
- ¹⁶R. Boehler, H. G. Musshoff, R. Ditz, G. Aquilanti, and A. Trapananti, *Rev. Sci. Instrum.* **80**, 045103 (2009).